Elastic and inelastic scattering of $^{58}Ni + ^{208}Pb$ at bombarding energies from 598 to 1011 MeV

M. Beckerman
Joint Institute for Heavy Ion Research and Oak Ridge National Laboratory, Oak Ridge, Tennessee 37831

R. L. Auble, F. E. Bertrand, J. L. Blankenship, B. L. Burks, M. A. G. Fernandes, C. W. Glover, E. E. Gross, D. J. Horen, R. O. Sayer, G. R. Satchler, D. Shapira, Y. Sugiyama,* and R. L. Varner
Oak Ridge National Laboratory, Oak Ridge, Tennessee 37831
(Received 16 March 1987)

High-resolution measurements have been made of elastic and inelastic scattering of $^{58}Ni + ^{208}Pb$ at four bombarding energies from 10.3 to 17.4 MeV/nucleon. The considerable inelastic strength observed for excitation energies up to at least 7 MeV is dominated by Coulomb-driven quadrupole transitions. Analyses were done using both the distorted-wave Born approximation and coupled-channels models. At the highest bombarding energies the data can be described equally well by distorted-wave Born approximations and coupled channels analyses. We find that $B(E2)=0.062\ e^2b^2$ for the 1.454 MeV 2^+ state in ^{58}Ni and $B(E2)=0.34\ e^2b^2$ for the 4.09 MeV 2^+ state in ^{208}Pb.

I. INTRODUCTION

Significant advances in our understanding of the physics of the interaction between two massive nuclei have occurred in the past few years as a result of measurements of subbarrier fusion.[1,2] From the fusion studies, from more recent studies of quasielastic transfer[3–5] and from accompanying theoretical investigation[6–10] we find that fusion, transfer, and inelastic scattering processes may profoundly influence one another, especially at energies in the vicinity of the classical Coulomb barrier.

Many questions remain outstanding concerning this interdependence of the various reaction channels. We find that there are as yet few detailed studies at any energy on transfer and elastic or inelastic scattering in massive systems. In this paper we present results of measurements and analyses of the elastic and inelastic scattering in the $^{58}Ni + ^{208}Pb$ system. Measurements of single neutron transfer have been made for this system as well and those results were presented in a recent publication.[11]

The measurements were made at energies from twice to 3.3 times the Coulomb barrier. Our objective was to obtain high resolution data against which detailed calculations using coupled-channel (CC) models and the distorted-wave Born approximation (DWBA) would be tested. By this means we hope to provide some understanding of the underlying reaction mechanisms and bring out differences and similarities between quasielastic (QE) reactions with massive projectiles and those involving light heavy ion and light ion projectiles.

Particular questions which we address involve assessing the relative importance of Coulomb and nuclear processes, and of coupling processes in such a system. We may note that the $^{58}Ni + ^{208}Pb$ system has an effective fissility slightly larger than those characterizing the systems used to form elements 107–109.[12] A study of the $^{58}Ni + ^{208}Pb$ system may provide insights into the failure to fuse in heavy systems and serve as a counterpoint for QE studies in less massive systems.

Inelastic scattering studies for massive ($A_p \geq 40$) systems have been reported previously for $^{40}Ar + ^{208}Pb$ at 236 keV (20% above the classical Coulomb barrier) (Ref. 13) and for $^{86}Kr + ^{208}Pb$ at 695 MeV (70% above the barrier).[14] Elastic scattering and inelastic scattering to the strongest low-lying states were studied. More detailed studies of heavy-ion inelastic scattering have been done in less massive systems, such as $^{16}O + ^{40}Ca$,[15–17] where a larger number of inelastic states can be resolved. In our study we examine the inelastic spectra up to 8 MeV. Our resolution is sufficient to allow a detailed examination of the strongly excited low-lying states and for information to be obtained from the angular distributions for the inelastic scattering to higher-lying unresolved states.

The paper is organized as follows. We begin with an overview of the experimental procedure, followed by description of the data so obtained. We next describe how the CC and DWBA analyses were done, and then present our results. We divide the spectra somewhat arbitrarily into two excitation regimes, discussing the states at low ($E_x < 4.5$ MeV) excitation first and then the states at high excitation. We end the paper with a comparison of our results to light-ion and electron scattering findings, and with a short summary.

II. EXPERIMENTAL PROCEDURE

In the experiments 598, 748, 913, and 1011 MeV beams of ^{58}Ni ions were provided by coupled cyclotron plus tandem operation at the Holifield Heavy Ion Research Facility (HHIRF). The ^{208}Pb targets were 50–100 $\mu g/cm^2$ thick on thin 15 $\mu g/cm^2$ carbon backings and isotopically enriched to 99.86%. Quasielastically scattered beamlike events were detected using the HHIRF broad-range magnetic spectrograph together with a microchannel plate "start" detector. Located in the focal plane of the magnetic spectrograph were a vertical drift chamber, an ion

chamber, and a parallel plate avalanche counter.[18] Elastic, inelastic and transfer products were completely resolved using time-of-flight (TOF), ΔE, E, and position signals from the detection system.

Up to three ionic charge states could be brought onto the focal plane for a given magnetic field setting. In order to minimize any errors arising from possible variations in detection efficiency, we made exclusive use of data for the peak charge state, which was positioned at the center of the focal plane. The full angular bite of the magnetic spectrograph was 3.8°, but measurements were carried out moving the spectrograph in 2° steps to give a broad angular overlap in successive measurements. The data were then sorted into 0.5° wide bins. Angular calibrations were done by measuring Rutherford scattering through a slitted mask. This allowed for a check of the software constants (e.g., drift velocity) used to determine position and angle. Data from the smallest and largest angle bins of a given setting were not included since edge effects were sometimes present. Small variations in efficiency due to wire plane geometry were corrected for.

Data were obtained in the above-mentioned manner in 0.5° bins from well inside to far beyond the grazing angle. Absolute cross sections were obtained by normalizing the yields to Rutherford scattering at forward angles. The beams were narrowly collimated using upstream slits and the target condition was checked by monitoring the scattering into a silicon surface barrier detector mounted at a forward angle in the scattering chamber. Beam currents on the targets were maintained at or below 1 particle nA to minimize target damage. The primary contributions to the energy resolution were finite beam-spot size and target inhomogeneities.

III. DATA

Displayed in Fig. 1 are ^{58}Ni energy spectra taken near the grazing angles at 598 and 1011 MeV. The energy resolution at 598 MeV was 600 keV. At 1011 MeV it is somewhat larger—on the order of 800 keV. We observe in Fig. 1 that there are several prominent structures in the inelastic spectra. Among these are well resolved peaks due to excitation of the first 2^+ state in ^{58}Ni at 1.454 MeV and excitation of the first 2^+ state in ^{208}Pb at 4.09 MeV. There are also smaller peaks in the spectra at 2.7 and 5.5 MeV.

The most detailed information was obtained at 1011 MeV. Less detailed information was obtained at 598 and 913 MeV. The statistics at 598 MeV were not sufficient to enable an equally detailed analysis over the entire spectra range. The 913 MeV data were acquired in an initial series of measurements with somewhat lower resolution and slightly poorer statistics than the 598 and 1011 MeV data.

Displayed in Fig. 2 are angular distributions at 1011 MeV corresponding to the various regions of excitation in the ^{58}Ni energy spectra. In this figure we observe an orderly progression of the shape of the angular distributions towards side peaking as the excitation increases. The magnitude of inelastic excitation is considerable, and as we will see shortly, is dominated by quadrupole transitions. The total cross sections for inelastic excitation up to 8 MeV obtained by integration over angle decreases slowly from 1200 mb at 598 MeV to 900 mb at 1011 MeV. These values are listed in Table I along with the reaction cross sections deduced from optical model and quarter-point analyses of the quasielastic data, as explained below.

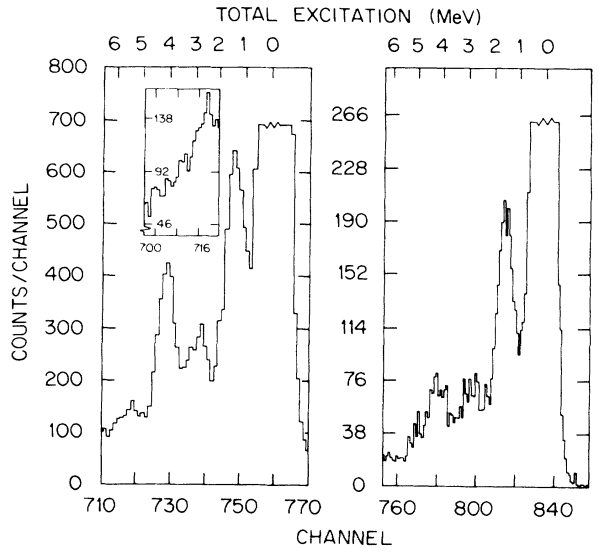

FIG. 1. Energy spectra at bombarding energies of 1011 MeV (left) and 598 MeV (right). Note the peaks at 1.45, 2.7, 4.1, and 5.5 MeV.

The 3_1^- (Pb), 2_3^+ (Ni), and 2_4^+ (Ni) states are located at 2.61, 3.03, and 3.26 MeV, respectively. These states were not completely resolved in the spectra. In the peak fitting analysis we made use of peak shapes and widths determined at each scattering angle from fitting the elastic peak. The most consistent fitting solution for the 2.6–3.3 MeV excitation energy region was obtained using a pair of peaks. One peak was placed at an excitation intermediate between those for the 3_1^- and 2_3^+ states and describes the sum of the cross sections for excitation of these states. The second peak was placed at an excitation energy just above that for the 2_4^+ state, and describes the remaining (2_4^+) strength below 3.9 MeV. A similar procedure was used for states in the 4.5–8.0 MeV region. In that excitation energy region we used three fitting peaks. The shapes for these peaks were determined at each scattering angle from appropriately broadened fits to the large peak at 4.1 MeV.

TABLE I. Cross sections.

Bombarding energy (MeV)	σ^{inel} (mb)	σ^{react} (mb)	σ^{total} (mb)
598	1200	3200	4400
913	975	4500	5475
1011	900	4600	5500

IV. REACTION MODEL CALCULATIONS

In the analyses of the data we employed a nuclear potential of Woods-Saxon form with volume absorption. Specifically,

$$V(r)=V_C(r)-Vf(r)-iWg(r) , \quad (1)$$

with a Coulomb potential given as

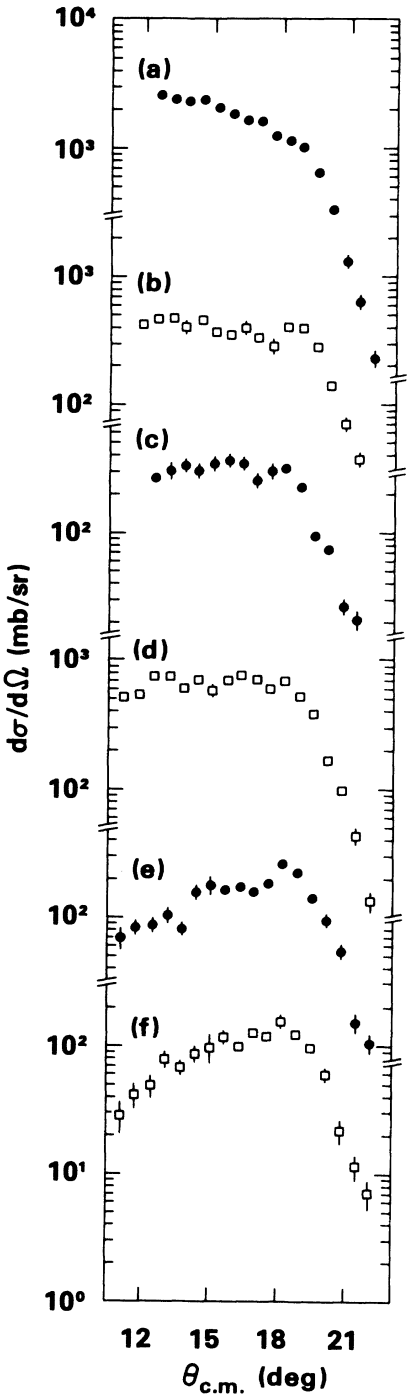

FIG. 2. Angular distributions for inelastic scattering obtained at 1011 MeV. Labeled (a)–(f) are the cross sections for inelastic scattering at excitations of 1.45, 2.7, 3.3, 4.1, 5.5, and 6.7 MeV.

$$V_C(r)=\begin{cases}\dfrac{Z_1Z_2e^2}{r}, & r\geq R_C\\ \dfrac{Z_1Z_2e^2}{2R_C}\left[3-\dfrac{r^2}{R_C^2}\right], & r<R_C\end{cases}$$

where $R_C=r_C(A_1^{1/3}+A_2^{1/3})=R_{1C}+R_{2C}$ and $r_C=1.2$ fm, and

$$f(r)=[1+e^{(r-R)/a}]^{-1}, \quad R=r_0(A_1^{1/3}+A_2^{1/3})=R_1+R_2 ,$$

$$g(r)=[1+e^{(r-R_I)/a_I}]^{-1}, \quad R_I=r_I(A_1^{1/3}+A_2^{1/3})$$
$$=R_{1I}+R_{2I} .$$

The coupling constant or form factors for inelastic excitation contain nuclear (hadronic) and Coulombic parts:

$$F_L(r)=F_L^C(r)+F_L^N(r) ,$$

with

$$F_L^C(r)=\begin{cases}4\pi Z_1e[B(EL)]^{1/2}/(2L+1)r^{L+1}, & r\geq R_C\\ 4\pi Z_1er^L[B(EL)]^{1/2}/(2L+1)R_C^{2L+1}, & r<R_C\end{cases}$$

and

$$F_L^N(r)=-\delta_L^{\mathrm{Re}}V\frac{df}{dr}-i\delta_L^{\mathrm{Im}}W\frac{dg}{dr} ,$$

where $\delta_L^{\mathrm{Re}}=\beta_L^{\mathrm{Re}}R_2$ and $\delta_L^{\mathrm{Im}}=\beta_L^{\mathrm{Im}}R_{2I}$ are real and imaginary deformation lengths. In the analyses we used the same deformation parameter β_L for both real and imaginary parts. In the above notation the subscript 2 denotes the nucleus being excited and 1 denotes the other nucleus. The quantity $B(EL)$ is the reduced electromagnetic rate for the upward transition, i.e., from the ground state (0^+) to the excited state ($0^+\rightarrow 2^+$, $0^+\rightarrow 3^-$, . . .). The Coulomb deformation parameters are defined from the $B(EL)$ values

$$\beta_C=\frac{4\pi}{3Z_2R_{2C}^L}[B(EL)]^{1/2} ,$$

and $\delta_C=\beta_CR_{2C}$ is the Coulomb deformation length.

Coupled-channel and DWBA analyses of the 598 and 1011 MeV data were done using the code PTOLEMY,[19] and a coupled-channel analysis of the 913 MeV data was performed using the code ECIS.[20] The starting point for the DWBA and coupled-channel analyses of the 598 and 1011 MeV data was an optical model analysis of the elastic data using, in addition to (1), an approximate dynamic polarization potential[21] to represent the long-range absorption due to Coulomb excitation. This polarization potential was characterized by an effective β_C describing the total inelastic strength and an average adiabaticity parameter g_λ. Values for these constants appropriate for our systems are listed in Table II together with deduced optical model parameters.

We observe in Fig. 3 that this approach gives an excellent description of the elastic data. (It also has been used in an analysis of the elastic scattering of $^{40}Ar+^{208}Pb$ at 236 MeV.[13]) The optical potentials for our systems so obtained were used in the analysis of the transfer data.[11] In our analyses we fixed the central real well depth, chose a

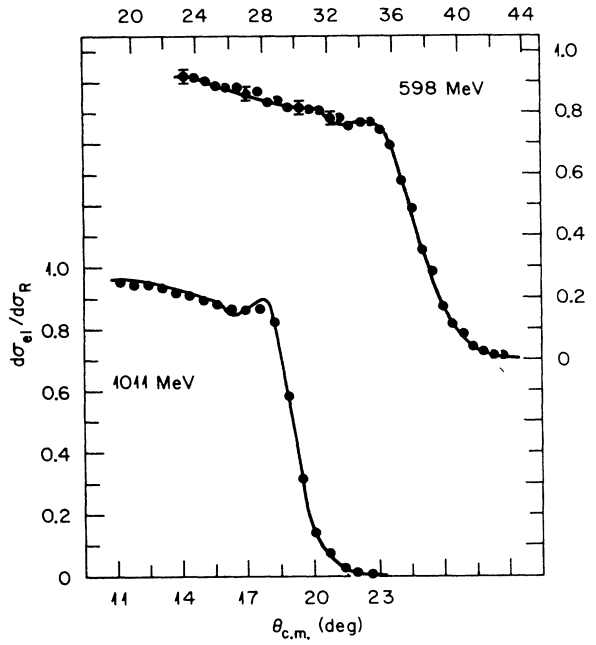

FIG. 3. Elastic scattering data plotted on a linear scale. Solid circles are the experimental results. Solid curves were obtained from optical model fits using the dynamic polarization potential.

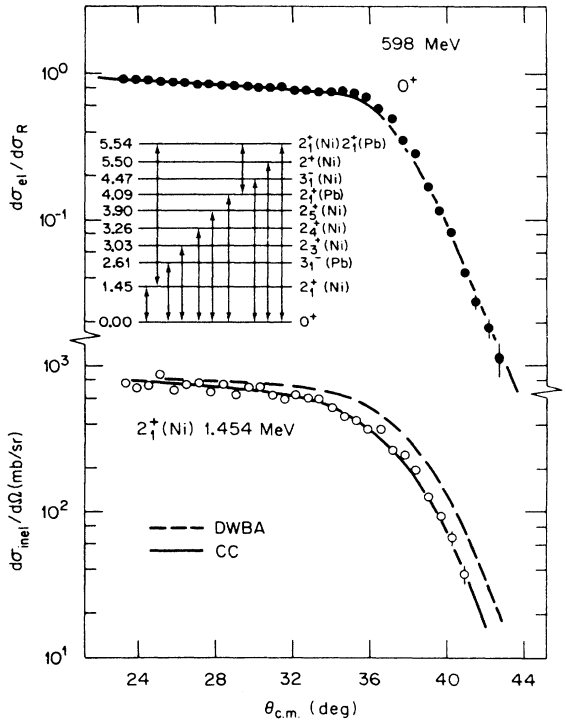

FIG. 4. Angular distributions for elastic and inelastic scattering. Solid and open circles denote experimental results for elastic scattering and for inelastic excitation of the 1.454 MeV 2^+ state in ^{58}Ni, respectively. Solid curves are coupled-channel predictions. The dashed curve indicates the corresponding DWBA prediction.

comparable central imaginary well depth, and varied the radii and diffusenesses. Up to 1300 partial waves were included in the calculations because of the long-range polarization potential (the grazing partial wave ranged from $L=320$ at 598 MeV to 500 at 1011 MeV).

These optical model parameter sets, without the Coulomb-excitation polarization potential, were used as a starting point for the coupled-channel analysis. (The Coulomb excitation is treated explicitly in the CC approach.) Included in the coupled channel calculations were those direct couplings between the elastic channel and the inelastic states shown schematically in Fig. 4, all treated as vibrations. For simplicity, we fixed $r_0=r_i$. The resulting optical potential that describes the elastic data in the presence of the coupling interactions is given in Table II together with the values of $Vf(R_{SA})$ and $Wg(R_{SA})$, with $R_{SA}=14.6$ fm (SA denotes strong absorption). Upon comparing these well depths to those obtained from our starting parameter set, we see that $Wg(R_{SA})$ is increased while $Vf(R_{SA})$ is fairly constant.

An alternative approach was taken for the 913 MeV data, where we employed a three channel model. In that analysis we focused our attention on the 1.45 MeV ^{58}Ni 2^+ state, and used an effective 2^+ state placed at 3 MeV to describe the rest of the 2^+ strength. Again, direct couplings to the elastic channel were considered as vibrations. A full parameter search was conducted. In this search, we started with shallower real and imaginary central well depths.

The cross sections listed in Table I in the column labeled σ^{react} do not include the inelastic contributions.

TABLE II. Optical model and polarization potential parameters used in the DWBA and coupled-channel calculations.

Bombarding energy (MeV)	V (MeV)	r_0 (fm)	a (fm)	W (fm)	r_I (fm)	a_I (fm)	β_C	g_λ	$Vf(R_{SA})$ (MeV)	$Wg(R_{SA})$ (MeV)
598	75.7	1.134	0.801	75.0	1.156	0.629	0.24	0.852	0.96	0.41
1011	75.7	1.144	0.805	75.0	1.093	0.872	0.24	0.980	1.10	0.85
598	105.0	1.163	0.680	70.0	1.163	0.730	coupled channels		0.93	0.85
1011	105.0	1.144	0.740	85.0	1.144	0.770	coupled channels		1.06	1.02
913	27.7	1.210	0.934	38.8	1.160	0.896	coupled channels		1.39	1.02

They may represent the reaction cross sections that would be deduced if the elastic and inelastic scattering were not resolved. These reaction cross sections were obtained by setting the polarization term to zero in the optical potential obtained from the optical model analysis of the elastic scattering. They were given in the coupled-channel analysis by the total absorption into all channels not included explicitly in the CC space. The cross sections listed in the table represent the average of these two methods (which differ by less than 5% from one another). The total reaction cross sections σ^{total} are the sum of these absorption cross sections and the inelastic cross sections for excitation energies up to 8 MeV. The total reaction cross sections listed in the table are the average of the values obtained in the optical model analysis of the fully resolved data, done using the polarization potential, and in the coupled-channel analysis from the coupled-elastic fits.

In the calculations there is an evolution towards side peaking on the part of the differential inelastic cross sections as the excitation energy increases consistent with that seen in the data. At forward scattering angles there is a substantial decrease in the elastic scattering below Rutherford values because of the absorption due to Coulomb excitation. This decrease is most clearly visible in the linear plots presented in Fig. 3. This absorption is generated in the optical model analysis by the long-range dynamic polarization term.

A measure of the strong absorption radius R_{SA} is given by the expression

$$kR_{\text{SA}}=\eta+(\eta^2+L_{\text{gr}}^2)^{1/2} ,$$

where k denotes the wave number, η is the Sommerfeld parameter, and L_{gr} represents the grazing L value defined here as the L for which the S-matrix element is $|S_L|^2=\frac{1}{2}$. With this definition $R_{\text{SA}}\approx 14.6$ fm at all three energies. The strength of the nuclear absorptive term, as represented by imaginary potential $W(r)$, increases as the bombarding energy increases; the depth of the imaginary potential at the strong absorption radius $R_{\text{SA}}=14.6$ fm changes from 0.41 MeV at 598 MeV to 0.85 MeV at 1011 MeV in the one channel optical-model (OM) analysis, or from 0.85 to 1.02 MeV in the CC analysis.

V. RESULTS

A. Coulomb and nuclear processes

The relative importance of Coulombic and nuclear processes can be seen in the plots presented in Fig. 5. Shown are results of calculations of pure Coulombic and pure nuclear excitation of several 2^+ states located at progressively higher excitation energies. The results were obtained using the distorted-wave Born approximation. The calculations of pure Coulomb excitations were made by setting the nuclear deformation lengths equal to zero, and the pure nuclear excitations were generated by setting the electromagnetic transition rates equal to zero.

For our mass (charge) -energy regime we find that the cross sections for Coulomb excitation dominate over those for nuclear excitation for almost the entire angular range

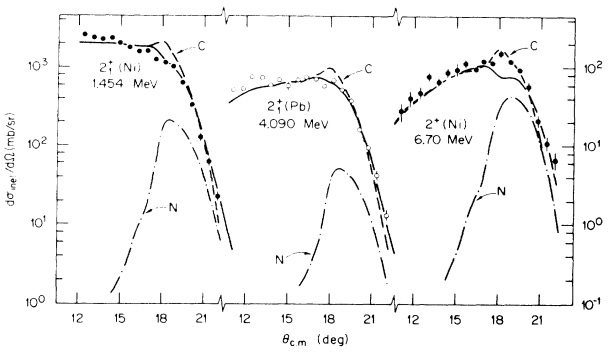

FIG. 5. Angular distributions. Open and solid circles denote experimental results. Smooth curves are DWBA predictions. Dashed-dotted: cross sections for nuclear excitation; dashed: cross sections for Coulomb excitation; solid: cross sections obtained from the full calculation.

even for transitions to high excitation energies. Thus, the $B(EL)$ values determine the overall magnitude of the inelastic scattering. They can be deduced unambiguously in a model independent way from the inelastic cross sections at small scattering angles. The nuclear interactions provide some destructive interference in the vicinity of the peak of the nuclear amplitude. At large scattering angles nuclear and Coulomb cross sections appear to interfere constructively.

The Coulomb dominance seen here in the $^{58}Ni+^{208}Pb$ system differs considerably from the behavior of, for example, the $^{16}O+^{44}Ca$ system at a bombarding energy of 60 MeV. For that system it was found[17] that while the cross section for excitation of the 1.156 MeV 2^+ state was dominated by Coulomb excitation, the cross section for excitation of the second 2^+ state at 2.656 MeV was dominated by nuclear excitation with Coulomb excitation an order of magnitude smaller.

In our DWBA and coupled-channel analyses we fixed the nuclear deformation lengths at about 90% of the value for the Coulomb deformation lengths. This convention gave satisfactory results and represents a compromise between the approaches of taking equal deformation lengths or using somewhat reduced nuclear values.[17]

B. States below 4.5 MeV

Displayed in Fig. 4 along with the elastic data are the measured and predicted cross sections for excitation of the 2^+ state in ^{58}Ni at 1.454 MeV. Both DWBA and coupled-channel results are given. The DWBA predictions are in good agreement with the data at forward angles but exceed the measured cross sections at large scattering angles. The coupled-channel results for the same $B(E2)$ and β_L values are in excellent agreement with the data over the entire angular range.

This situation changes at the higher bombarding energies. At 1011 MeV, as shown in Fig. 6, the DWBA and CC predictions for excitation of the 1.454 MeV 2^+ state are virtually identical over the entire angular range. Although the "bare" optical potentials used in conjunction

with the dynamic polarization potential and with the coupled channels differ, this equality occurs provided the elastic scattering is reliably described.

The coupled channel predictions for excitation of the 1.454 MeV state at 913 MeV are displayed in Fig. 7. The deformation parameter $\beta_C = 0.173$ deduced in the three channel model is identical to that deduced at 1011 MeV using the more detailed set of coupled channels and using the DWBA. The deformation parameter for the virtual 2^+ state is $\beta_C = 0.170$. Combining the two deformation parameters in quadrature yields the value 0.24 used as the effective β_C in the dynamic polarization approach to describe the elastic scattering.

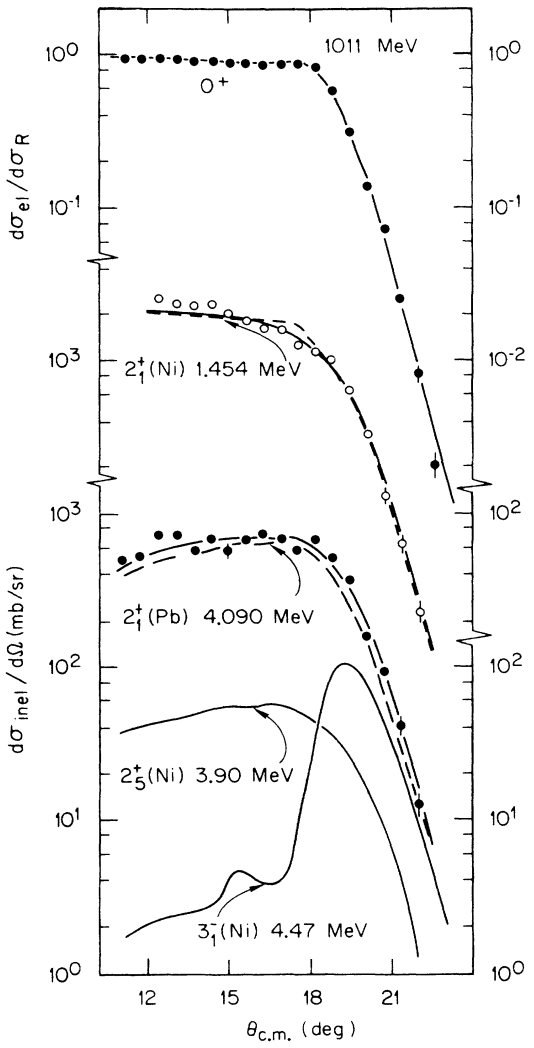

FIG. 6. Angular distributions for elastic and inelastic scattering. Open and solid circles show experimental cross sections. Smooth curves represent model results. Upper panel: elastic scattering. Middle panel: inelastic excitation of the 1.454 MeV 2^+ state in ^{58}Ni. Solid curve gives the coupled-channel result; dashed curve denotes the DWBA prediction. Lower; inelastic excitation of the 4.090 MeV 2^+ state in ^{208}Pb. Uppermost solid curve represents the coherent sum of cross sections for inelastic excitation of the 4.090 MeV 2^+ state, the 4.47 MeV 3^- state in ^{58}Ni [$B(E3) = 0.0171\ e^2b^3$], and the 3.90 MeV 2^+ state in ^{58}Ni [$B(E2) = 0.0030\ e^2b^2$].

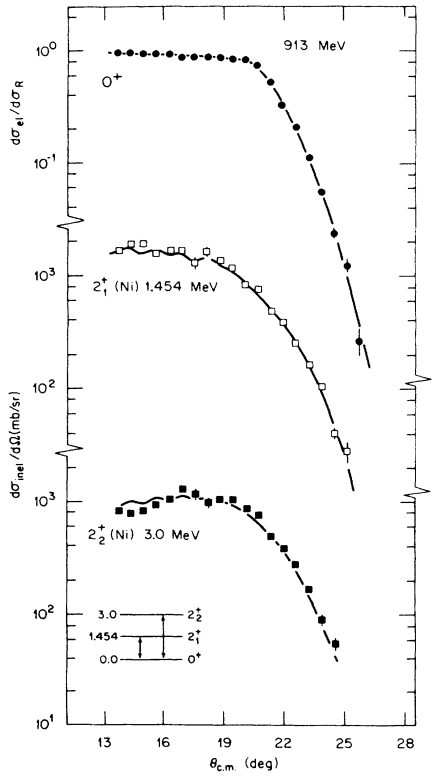

FIG. 7. Angular distributions for elastic and inelastic scattering. Open and solid symbols give the experimental results. Smooth curves denote coupled-channel predictions. Upper: elastic scattering. Middle: inelastic excitation of the 1.454 MeV 2^+ state in ^{58}Ni. Lower; inelastic excitation of a fictitious 2^+ state at 3.0 MeV representing the remaining inelastic strength.

Coupled-channel calculations for the excitation of the 2^+ state in ^{208}Pb at 4.090 MeV are compared to the data in Fig. 6. Included in the experimental results are contributions from the 2^+_5 state in ^{58}Ni at 3.90 MeV and the 3^-_1 state in ^{58}Ni at 4.47 MeV. The contributions from these unresolved states are predicted to be small; calculated using electromagnetic transition rates and deformation lengths from the literature,[22–27] they are predicted to be in the range 10–20 % of the total. The $B(E2)$ value deduced from our analyses for the 4.090 MeV state is listed in Table III. As was the case for the 1.454 MeV state, both DWBA and CC predictions are nearly identical.

We have already observed some of the consequences of Coulomb-driven quadrupole dominance on the inelastic scattering. The 2^+_3 and 2^+_4 states in ^{58}Ni are located at 3.03 and 3.26 MeV, respectively. Electromagnetic transition rates for these "weak" states have been determined from electron scattering measurements,[23] and deformation lengths δ_L have been deduced from light ion studies.[24] DWBA and CC calculations of the cross sections for excitation of these states are presented in Fig. 8 together with the cross sections for exciting the very collective 3^- state in ^{208}Pb at 2.61 MeV.[27] We observe that the 2^+ cross

TABLE III. Electromagnetic transition rates and Coulomb deformation constants deduced in this work.

E_x (MeV)	Bombarding energy (MeV)	$B(E2)$ (e^2b^2)	δ_C (fm)	β_c
1.454	1011	0.0620	0.802	0.173
	913	0.0622	0.804	0.173
	598	0.0570	0.769	0.166
4.090	1011	0.342	0.420	0.059

sections are comparable in magnitude to those for the 2.61 MeV 3^- state, and there is good agreement between the data and the model calculations. It is noteworthy that in the case of the "weak" 2^+ states the DWBA and CC approaches yield nearly identical results. Large departures of the DWBA predictions from experimental results at large scattering angles have been reported[17] in the past for the case of weak states in less massive systems at lower energies, where the nuclear contributions play a stronger role.

C. States from 4.5 to 8.0 MeV

The angular distribution for excitation of states near 5.5 MeV is plotted in Fig. 9. Part of the yield at 5.5 MeV can be ascribed to the mutual excitation of the 1.454 MeV 2^+ state in ^{58}Ni and the 4.09 MeV 2^+ state in ^{208}Pb. In addition, there is a 2^+ state in ^{208}Pb at 5.564 MeV with a $\beta_2=0.017$, and there is a state in ^{58}Ni at 5.50 MeV identified by Bruge *et al.*[24] as a 2^+ state and by Jarvis *et al.*[25] as a 4^+ state.

Shown in Fig. 9 are the predicted cross sections for mutual excitation of the first 2^+ states of the target and projectile. Included in the calculations are the contributions from both simultaneous and sequential excitation. Upon examining the separate contributions for these two processes, we find that sequential excitation is far more likely (by about a factor of 6 or 7) than simultaneous excitation. This may be contrasted to the behavior observed[28] in the Coulomb/nuclear interference region for the $^{28}Si+^{58}Ni$ system where these processes were found to be comparable in magnitude.

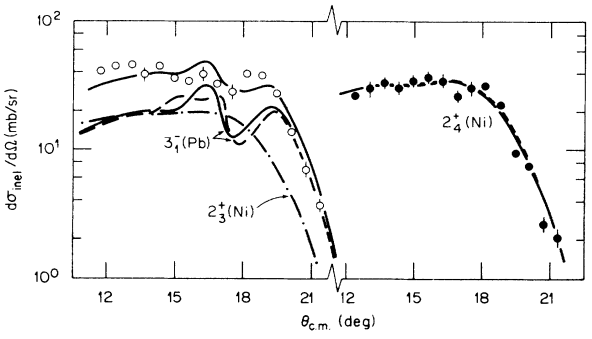

FIG. 8. Angular distributions for inelastic scattering at 1011 MeV. Left: open circles give the experimental cross sections for the states near 2.7 MeV. Dashed-dotted curve shows the coupled-channel prediction for the 2^+ state in ^{58}Ni at 3.03 MeV [$B(E2)=0.0083$ e^2b^2]. Solid and dashed curves give the coupled-channel and DWBA predictions for the 3^- state in ^{208}Pb at 2.61 MeV [$B(E3)=0.741$ e^2b^3]. Upper smooth curve shows the sum of 2^+ and 3^- cross sections. Right: circles show the experimental results for the state near 3.3 MeV. Solid and dashed curves denote coupled-channel and DWBA predictions for the 2^+ state in ^{58}Ni at 3.26 MeV [$B(E2)=0.0153$ e^2b^2].

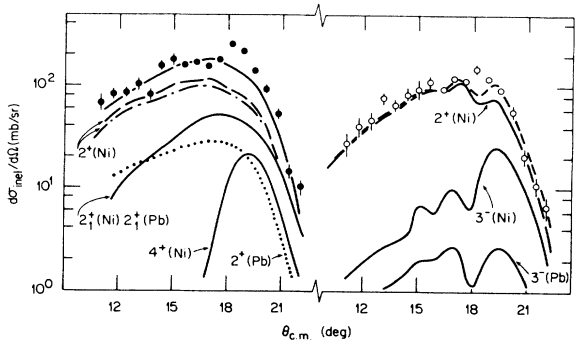

FIG. 9. Angular distributions for inelastic scattering at 1011 MeV. Left: solid circles show experimental cross sections for states at an apparent excitation of 5.5 MeV. Dotted curves give the DWBA predictions for the 5.564 MeV 2^+ state in ^{208}Pb [$B(E2)=0.026$ e^2b^2]. Solid curves labeled 2^+ and 4^+ denote DWBA predictions for 2^+ and 4^+ states in ^{58}Ni at 5.50 MeV. The dashed-dotted curve gives the corresponding coupled-channel prediction for the 2^+ state [$B(E2)=0.0120$ e^2b^2; $B(E4)=0.000\,453$ e^2b^4; $\beta_2=0.070=\beta_4$]. Curve labeled 2^+2^+ shows the coupled-channel prediction for the mutual excitation of the first excited 2^+ states. Uppermost smooth curve represents the coherent sum of cross sections for the 2^+ (Ni) and 2^+ (Pb) states and the cross section for the mutual excitation of the 2_1^+ (Ni) and 2_1^+ (Pb) states. Right: open circles give the total cross sections for the excitation energy region center at 6.70 MeV. Solid curves labeled 3^- (Pb) and 3^- (Ni) give DWBA predictions for the 6.62 MeV 3^- state in ^{208}Pb [$B(E3)=0.0129$ e^2b^3] and the 6.7 MeV states in ^{58}Ni [$B(E3)=0.004\,25$ e^2b^3]. Solid curve labeled 2^+ gives the cross sections for an effective 2^+ state at 6.70 MeV having a $\delta_C=0.096$ fm. Dashed curve gives the coherent sum.

Also displayed in Fig. 9 are the calculated cross sections for excitation of the 5.564 MeV 2^+ state, and for the excitation of 2^+ and 4^+ states in ^{58}Ni of comparable deformation lengths. The angular distributions corresponding to transitions of different multipolarities are quite different at these excitation energies. The magnitude of the cross sections at forward scattering angles is consistent with the presence of a 2^+ state in ^{58}Ni near 5.50 MeV having a $B(E2)$ on the order of the value given by Bruge *et al.*, so that the overall shape of the measured angular distribution is consistent with that given by the sum of mutual excitation and the known ^{58}Ni and ^{208}Pb 2^+ cross sections, although there are discrepancies between data and predictions in the 17°–19° region.

Also displayed in Fig. 9 is the angular distribution for inelastic scattering over a broad excitation energy region centered near 6.7 MeV. We find that the inelastic scatter-

ing cross sections at these excitation energies are appreciable, and although there are no clearly discernible peaks in the spectra, the inelastic strength seen near 6.7 MeV continues up to at least 8 MeV.

Several 3^- states have been identified[24] in the vicinity of 6.7–6.8 MeV in ^{58}Ni and there is a 3^- state in ^{208}Pb at 6.6 MeV.[29] These octupole excitations can account for about 30% of the inelastic strength near the maximum in the angular distribution. As was the case for excitation of the 3^- state in ^{208}Pb at 2.61 MeV and the 3^- state in ^{58}Ni at 4.47 MeV, excitation of 3^- states near 6.7 MeV can account for only a small part of the observed forward angle yield. We can reproduce the experimental cross sections by adding to the 3^- results those corresponding to the inelastic excitation of one or more as yet unidentified 2^+ states whose sum can be characterized by an effective deformation length $\delta_{\text{eff}}=0.40$ fm.

In their ^{208}Pb(e,e') study Ziegler and Peterson[30] find a strong 2^+ state at 6.2 MeV with a $B(E2)=0.070\ e^2b^2$. Hicks *et al.*[31] report a value of 0.0505 e^2b^2 for this state, while Frey[29] gives the value 0.0526 e^2b^2. Using the larger $B(E2)$, we calculate that excitation of such a 6.2 MeV 2^+ state would account for about 40% of our measured forward angle cross sections.

Other 2^+ states have been seen in (e,e') measurements at 6.367 and 7.344 MeV by Frey.[29] However the $B(E2)$ values are small, on the order of 0.0042 and 0.0215 e^2b^2, respectively. In a high resolution ^{208}Pb(p,p') study, Fujita *et al.*[32] find considerable 2^+ strength at excitation energies from 7.28 to 7.46 MeV. We estimate that about half of the remaining strength in the excitation energy region centered at 6.7 MeV may arise from inclusion of a portion of this higher-lying strength. The total strength observed by us in the 6.0–8.0 MeV range, if quadrupole in character and restricted to ^{208}Pb, is about 12% of the energy-weighted sum rule (EWSR) limit.

D. Discussion of 1.454 and 4.090 MeV states

Deformation lengths for the 1.454 MeV 2^+ state have been deduced previously from measurements of light ion inelastic scattering, sub-Coulomb heavy ion scattering, and electron scattering. The nuclear deformation lengths deduced from (p,p'), (^{3}He,^{3}He'), and (α,α') reactions tend to cluster about a value $\delta_L=1.0$ fm,[22] as does the result of Bruge *et al.*,[24] which yielded a value of $\delta_L=0.95$ fm. In contrast to the light ion findings, values for δ_C extracted from heavy ion sub-Coulomb measurements average about 0.80 fm,[22] as does our result. Listed in Table IV are results for $B(E2)$ deduced from sub-Coulomb and (e,e') measurements. The $B(E2)$ we extract is also consistent with the electron scattering values. (We have $\beta_C=0.173$, while Duguay *et al.*[23] find $\beta_C=0.177$.)

Values for $B(E2)$ for the 4.090 MeV 2^+ state in ^{208}Pb are given in Table IV. Our result is slightly higher than the average of the electron scattering values, and is somewhat lower than the $B(E2)$'s extracted from δ_L in a model-dependent manner by Morsch *et al.*[37] Nuclear deformation lengths have been deduced in several (p,p') and (α,α') studies. Scott *et al.*[38] find $\beta_L=0.055$ as does Alster.[39] Results from (p,p') measurements have been tabulated in Refs. 38, 40, and 41. Those values vary from 0.050 to 0.060. The value for β_L used by us was $\beta_L=0.056$ (recall we set $\delta_L=0.9\delta_C$).

Several heavy ion inelastic scattering studies have been carried out in the Coulomb-nuclear interference region. The values for β_L tend to exceed slightly the value deduced in our study. Ford *et al.*[42] find from their analysis of (^{11}B,^{11}B') scattering that $\beta_L=0.060$ (giving $\delta_L=0.476$ fm),and most recently[43] a coupled-channel analysis of (^{28}Si,^{28}Si') scattering yielded the resulting $\delta_L=0.43$ fm. However, in making these comparisons we stress that there is no fundamental requirement that the simple deformed optical potential models should provide invariant deformation lengths or deformation parameters. In principle, these quantities may depend on the probe and associated optical potentials.

VI. SUMMARY

In this work we investigated the inelastic scattering of ^{58}Ni + ^{208}Pb at several energies from twice to 3.3 times the Coulomb barrier. The most striking feature of the inelastic scattering process is the strong Coulomb dominance. As a consequence of this dominance we find that the cross sections for excitation of 2^+ states are greatly enhanced over those for excitation of states of higher multipolarity.

TABLE IV. Comparison of $B(E2)$ results for the 1.454 MeV 2_1^+ state in ^{58}Ni and the 4.090 MeV 2_1^+ state in ^{208}Pb.

State (MeV)	$B(E2)$ (e^2b^2)	Ref.	State (MeV)	$B(E2)$ (e^2b^2)	Ref.
1.454	0.0657	a	4.090	0.296	f
	0.0554	b		0.318	g
	0.066	c		0.350	h
	0.0726	d		0.370	j
	0.0621	e		0.342	e

[a]Reference 23, (e,e').
[b]Reference 33, (e,e').
[c]Reference 34, sub-Coulomb.
[d]Reference 35, sub-Coulomb.
[e]Present work.
[f]Reference 30, (e,e').
[g]Reference 36, (e,e').
[h]Reference 37, (d,d').
[i]Reference 37, (α,α').

At the highest bombarding energies we find that the coupled-channel models and the distorted-wave Born approximation give almost identical inelastic scattering predictions. This happens for both weakly and strongly excited states.

Quadrupole strength is observed at excitations up to 8 MeV. In the range 6.0–8.0 MeV, we estimate that the observed strength exhausts about (12±2)% of the EWSR for ^{208}Pb. The Coulomb selectivity allows us to deduce $B(E2)$ values unambigiously for the strongly excited 2^+ states. At the higher bombarding energies there is little sensitivity to model assumptions and other accompanying parameters. We find $B(E2)=0.062\ e^2b^2$, $\delta_C=0.80$ fm, and $\beta_C=0.173$ for the 1.454 MeV 2^+ state in ^{58}Ni, and $B(E2)=0.34$, e^2b^2, $\delta_C=0.42$ fm, and $\beta_C=0.059$ for the 4.090 MeV 2^+ state in ^{208}Pb.

ACKNOWLEDGMENTS

The Joint Institute for Heavy Ion Research is supported by its member institutions and by the U.S. Department of Energy under Contract No. DE-AS05-76ER0-4936 with the University of Tennessee. Oak Ridge National Laboratory is operated by Martin Marietta Energy Systems, Inc., under Contract No. DE-AC05-84OR21400 with the U.S. Department of Energy. One of us (Y.S.) was on assignment to the Physics Division of Oak Ridge National Laboratory (ORNL) under a cooperative research agreement between the Japan Atomic Energy Research Institute (JAERI) and Martin Marietta Energy Systems, Inc. He would like to thank the Japan Atomic Energy Research Institute and Oak Ridge National Laboratory for support during his stay in Oak Ridge.

*Present address: Japan Atomic Energy Research Institute, Tokai, Ibaraki 319-11, Japan.

[1]M. Beckerman, Phys. Rep. **129**, 145 (1985).

[2]*Proceedings of the International Conference on Fusion Reactions below the Coulomb Barrier*, Cambridge, Mass., 1984, edited by S. G. Steadman (Springer-Verlag, Berlin, 1985).

[3]K. E. Rehm, F. L. H. Wolfs, A. M. van den Berg, and W. Henning, Phys. Rev. Lett. **55**, 280 (1985); J. Wiggins, R. Brooks, M. Beckerman, S. B. Gazes, L. Grodzins, A. P. Smith, S. G. Steadman, Y. Xiao, and F. Videbaek, Phys. Rev. C **31**, 1315 (1985).

[4]Y. Sugiyama, Y. Tomita, H. Ikezoe, K. Ideno, N. Shikazono, N. Kato, H. Fujita, T. Sugimitzu, and S. Kubono, Phys. Lett. **176B**, 302 (1986).

[5]A. M. van den Berg, W. Henning, L. L. Lee, Jr., K. T. Lesko, K. E. Rehm, J. P. Schiffer, G. S. F. Stephans, F. L. H. Wolfs, and W. S. Freeman, Phys. Rev. Lett. **56**, 572 (1986).

[6]C. H. Dasso, S. Landowne, and A. Winther, Nucl. Phys. **A405**, 381 (1983).

[7]S. Landowne and S. C. Pieper, Phys. Rev. C **29**, 1352 (1984).

[8]M. J. Rhoades-Brown and P. Braun-Munzinger, Phys. Lett. **136B**, 19 (1984).

[9]R. A. Broglia, C. H. Dasso, S. Landowne, and G. Pollarolo, Phys. Lett. **133B**, 34 (1983).

[10]C. Mahaux, H. Ngô, and G. R. Satchler, Nucl. Phys. **A449**, 354 (1986).

[11]M. Beckerman, R. L. Auble, F. E. Bertrand, J. L. Blankenship, B. L. Burks, C. W. Glover, R. O. Sayer, G. R. Satchler, D. Shapira, and R. L. Varner, Phys. Rev. Lett. **58**, 455 (1987).

[12]P. Armbruster, Annu. Rev. Nucl. Part. Sci. **35**, 135 (1985).

[13]U. Arlt, R. Bass. V. Hartmann, R. Renfordt, K. Sapotta, P. Fröbrick, and W. Schäfer, Phys. Rev. C **22**, 1790 (1980).

[14]J. Cheng-Lie, P. R. Christensen, Ole Hansen, S. Pontoppidan, F. Videbaek, D. Schull, S. Wen-Qing, A. S. Baltz, P. D. Bond, and H. Freiesleben, Phys. Rev. Lett. **47**, 1039 (1981).

[15]K. E. Rehm, W. Henning, J. R. Erskine, and D. G. Kovar, Phys. Rev. Lett. **40**, 1479 (1978).

[16]R. J. Ascuitto, J. F. Petersen, and E. A. Segele, Phys. Rev. Lett. **41**, 1159 (1978).

[17]K. E. Rehm, W. Henning, J. R. Erskine, D. G. Kovar, M. H. Macfarlane, S. C. Pieper, and M. Rhoades-Brown, Phys. Rev. C **25**, 1915 (1982).

[18]J. L. C. Ford, Jr., R. L. Auble, F. E. Bertrand, J. L. Blankenship, T. P. Sjoreen, E. E. Gross, R. O. Sayer, and D. Shapira, Oak Ridge National Laboratory, Physics Division Progress Report ORNL-6004, 1983, p. 147; M. V. Hynes, J. L. C. Ford, Jr., T. P. Sjoreen, J. L. Blankenship, and F. E. Bertrand, Nucl. Instrum. Methods **224**, 89 (1984); T. P. Sjoreen, J. L. C. Ford, Jr., J. L. Blankenship, R. L. Auble, F. E. Bertrand, E. E. Gross, D. C. Hensley, D. Schull, and M. V. Hynes, *ibid.* **224**, 421 (1984).

[19]M. H. Macfarlane and S. C. Pieper, Argonne National Laboratory Report No. ANL-76-11, (Rev. 1), 1978; M. J. Rhoades-Brown, S. C. Pieper, and M. H. Macfarlane, Phys. Rev. C **21**, 2417 (1980).

[20]J. Raynal, CEN-Saclay Report DPh-T/7148, 1971; Phys. Rev. C **23**, 2571 (1981).

[21]W. G. Love, T. Terasawa, and G. R. Satchler, Nucl. Phys. **A291**, 183 (1977).

[22]A. M. Bernstein, Adv. Phys. **3**, 325 (1969).

[23]M. A. Duguay, C. K. Bockelman, T. H. Curtis, and R. A. Einstein, Phys. Rev **163**, 1259 (1967).

[24]G. Bruge, A. Chaumeaux, R. DeVries, and G. C. Morrison, Phys. Rev. Lett. **29**, 295 (1972).

[25]O. N. Jarvis, B. G. Harvey, D. L. Hendrie, and J. Mahoney, Nucl. Phys. **A102**, 625 (1967).

[26]G. Bruge, J. C. Faivre, H. Faraggi, and A. Bussiere, Nucl. Phys. **A146**, 597 (1970).

[27]J. S. Lilley, M. A. Franey, and D. H. Feng, Nucl. Phys. **A324**, 165 (1980).

[28]P. D. Bond, Ole Hansen, C. E. Thorn, M. J. LeVine, R. P. Christensen, S. Pontoppidan, F. Videbaek, J. C. Lie, and M. J. Rhoades-Brown, Phys. Lett. **114B**, 423 (1982).

[29]R. W. Frey, Ph.D. dissertation, Technische Hochschule Darmstadt, 1978; M. J. Martin, Nucl. Data Sheets **47**, 797 (1986).

[30]J. F. Ziegler and G. A. Peterson, Phys. Rev. **165**, 1337 (1968).

[31]R. S. Hicks, R. L. Huffman, R. A. Lindgren, B. Parker, G. A. Peterson, S. Raman, and C. P. Sargent, Phys. Rev. C **26**, 920 (1982).

[32]Y. Fujita, M. Fujiwara, S. Morinobu, I. Katayama, T. Yamazaki, T. Itahashi, H. Ikegami, and S. I. Hayakawa, Phys. Rev. C **32**, 425 (1985).

[33]V. D. Afans'ev, N. G. Afans'ev, I. S. Gul'karov, G. A. Sav-

itskii, V. M. Khvastunov, N. G. Shevchenko, and A. A. Khomich, Yad. Fiz. **10**, 33 (1969) [Sov. J. Nucl. Phys. **10**, 18 (1970)].
[34]P. R. Christensen, I. Chernov, E. E. Gross, R. Stokstad, and F. Videbaek, Nucl. Phys. **A207**, 433 (1973).
[35]P. M. Lesser, D. Cline, and J. D. Purvis, Nucl. Phys. **A151**, 257 (1970).
[36]M. M. Gazzaly, N. M. Hintz, G. S. Kyle, R. K. Owen, G. W. Hoffmann, M. Barlett, and G. Blampied, Phys. Rev. C **25**, 408 (1982).
[37]H. P. Morsch, C. Sükösd, M. Rogge, P. Turek, H. Machner, and C. Mayer-Böricke, Phys. Rev. C **22**, 489 (1980).
[38]A. Scott, N. P. Mathur, and F. Petrovich, Nucl. Phys. **A285**, 222 (1977).
[39]J. Alster, Phys. Lett. **25B**, 459 (1972).
[40]W. T. Wagner, G. M. Crawley, G. R. Hammerstein, and H. McManus, Phys. Rev. C **12**, 757 (1975).
[41]D. K. McDaniels, J. Lisantti, L. W. Swenson, X. Y. Chen, D. J. Horen, F. E. Bertrand, E. E. Gross, C. Glover, R. Sayer, B. L. Burks, O. Hausser, and K. Hicks, Phys. Rev. C (in press).
[42]J. L. C. Ford, Jr., K. S. Toth, D. C. Hensley, R. M. Gaedke, P. J. Riley, and S. T. Thornton, Phys. Rev. C **8**, 1912 (1973).
[43]P. R. Christensen, S. Pontoppidan, F. Videbaek, J. Barrette, P. D. Bond, Ole Hansen, and C. E. Thorn, Phys. Rev. C **29**, 455 (1984).